

---

# Phase-unwrapping method based on phase-gradient estimation and energy equation

<sup>1</sup> Man Yan, <sup>2</sup> Juanjuan Luo and <sup>3</sup> Defa Hu

<sup>1</sup> Media and Communications College, Weifang University, Weifang 261061, Shandong, China

<sup>2</sup> Hunan International Economics University, Changsha 410205, Hunan, China

<sup>3</sup> Hunan University of Technology and Business, Changsha 410205, Hunan, China

**Received:** 15.06.2022

**Abstract.** Phase unwrapping is a key step in processing interferometric synthetic-aperture radar (InSAR) data. Here we offer a phase-unwrapping method based on phase-gradient estimation and energy equation. The method can be implemented through adjusting four neighbourhoods in the original energy-equation method to eight neighbourhoods and combining fast Fourier transform with chirp-Z transform for the estimation of phase gradient in iterative equation. Both simulated and real InSAR data are used to perform phase-unwrapping experiments. We test our phase-unwrapping method based on the phase-gradient estimation and the energy equation using such quantitative standards as, e.g., discontinuity map and root mean-square error. On this basis we compare our approach with some other standard phase-unwrapping methods. It is shown that our method suppresses efficiently the errors generated in unwrapping process and provides reliable and high-accuracy unwrapping results.

**Keywords:** interferometric synthetic-aperture radars, phase unwrapping, energy equation, phase-gradient estimation

**UDC:** 621.396.96+528

## 1. Introduction

Phase unwrapping is a key step in synthetic-aperture radar interferometry. Since formulation of the principles of interferometric synthetic-aperture radars (InSARs) in 1974, a number of phase-unwrapping methods have been developed. Each of these methods has its own characteristics, advantages and shortcomings. Let us define a phase residue as a point where the sum of differences for four adjacent pixel points is greater than zero. Then the phase-unwrapping methods can be divided into two main categories, depending on the phase-residue processing:

(1) Path-following phase-unwrapping methods. This category includes mainly a branch-cut method [1, 2], a minimum-spanning tree method [3], a region-growing method [4], a quality-map guided method [5], a mask-cut method [6], and a Flynn-minimum discontinuity one [7]. Their advantages are fast calculations and less memory requirements. However, the methods can easily impose error propagation during phase unwrapping, since one must ‘pass through’ rather than ‘bypass’ the phase residues.

(2) Non-path-following phase-unwrapping methods. They include a minimum-norm method [8–10], an optimal-estimation method [11, 12], a feature-extraction method [13, 14], an energy-equation method [15] and some others. These techniques do not need identification of phase residues in the phase-unwrapping process, the errors caused by the phase residues are avoided, while the unwrapping precision is high enough. Note that the phase-unwrapping method based upon the energy equation implies that an unwrapped constraint is converted into some energy function and then minimized.

However, when a terrain is steep or the relevant slope is relatively large, the phase jump  $2\pi$  often may cause some unwrapping errors which propagate from one pixel to its neighbours.

Among the previous work on the subject, one can remind the study by Liming Pu et al. [16] who have suggested a phase-gradient estimation network for the InSAR, which is based on encoder–decoder architecture PGENet. On the other hand, Xianming Xie et al. [17] have used an enhanced local phase-gradient estimator based on amended matrix-pencil model. Weike Liu et al. [18] have applied additional constraint condition to a nonlinear least-squares phase unwrapping in order to obtain a real phase. In the present work, we offer a phase-unwrapping method following from the energy equation and the phase-gradient estimation. First, four neighbourhoods in the original energy-equation phase-unwrapping method are adjusted to eight neighbourhoods. Then a fast Fourier transform (FFT) and a chirp-Z transform (CZT) are combined for phase-gradient estimating and phase unwrapping. Simulated data and real InSAR data are used for our experiments which verify feasibility and efficiency of this algorithm.

The remainder of this article is organized as follows. Section 2 introduces details of the phase-gradient estimation technique and our phase-unwrapping method, which is based on this approach and energy equalization. Section 3 illustrates performance of our method with the examples involving both simulated and real data. Here we also compare our method with its contemporary counterparts, including such representative algorithms as the network-flow and least-squares approaches. Finally, the concise conclusions are drawn in Section 4.

## 2. Description of the method

### 2.1. Phase-gradient estimation

In the two-dimensional phase unwrapping, practical signals are often non-stationary, so that the notion of frequency loses its usefulness. Then a parameter called as instantaneous frequency (IF) is usually introduced, which accounts for time-varying nature of the process. Note that the IF of the phase corresponds to the phase gradient. In general, a complex signal  $Z(x, y)$  in two-dimensional space can be represented as follows:

$$Z(x, y) = |Z(x, y)|e^{i\angle Z(x, y)} = |Z(x, y)|e^{iW[\phi(x, y)]}. \quad (1)$$

In Eq. (1),  $W[\phi(x, y)]$  is the principal value of the unwrapped (unknown) phase function  $\phi(x, y)$  and  $\angle Z(x, y)$  denotes the argument of the complex signal  $Z(x, y)$ . The unwrapped-phase surface  $\phi(x, y)$  can be derived from the IF of the phase. The IF estimated directly from the two-dimensional signal  $Z(x, y)$  is given by

$$\overline{f}^Z(x, y) = \nabla[\angle Z(x, y)] = f_x^Z(x, y)\overline{1}_x + f_y^Z(x, y)\overline{1}_y, \quad (2)$$

where  $\overline{f}^z$  implies the IF estimated from  $Z(x, y)$ ,  $\nabla$  is the gradient operator,  $f_x^z$  and  $f_y^z$  are respectively the  $x$  and  $y$  components of the estimated IF, and  $\overline{1}_x$  and  $\overline{1}_y$  mean the unit vectors respectively along the  $x$  and  $y$  directions.

The common frequency-estimation methods include (i) a method based on auto-correlation matrix, (ii) a multi-resolution method, which actually introduces multi-resolution idea into the auto-correlation matrix method and aims to eliminate aliasing errors, and (iii) a spectrum-estimation method. It is obvious that the spectrum-estimation method based on the FFT needs much time to achieve high estimation accuracy. On the other hand, high-precision estimation

results can be obtained quickly when introducing the CZT. As a result, below we will combine the FFT and CZT approaches to implement the frequency-estimation method.

## 2.2. Frequency-estimation approach based on combination of FFT and CZT

The core idea of the frequency estimation is that the phase within a small window can be simulated by the two-dimensional linear phase model. In other terms, the phase within this window can be regarded as having a single frequency. The appropriate mathematical model can be expressed as

$$\exp[j\phi(m, n)] = \exp(j\phi_0) \exp[j2\pi(mf_x + nf_y)], \quad (3)$$

where  $\phi(m, n)$  is the phase defined at the point within a given window (its displacement relative to the centre of the window being determined by  $(m, n)$ ),  $\phi_0$  denotes the average phase within the window, and  $f_x$  and  $f_y$  are the local frequencies associated respectively with the  $x$  and  $y$  directions.

As mentioned above, we combine the two-dimensional FFT and the CZT for estimating the local interference-fringe frequency. The basic idea of this method lies in the following. For the  $M \times N$  interferogram  $z(x, y)$ , the local fringe frequencies  $f_x$  and  $f_y$  at the point  $(x, y)$  can be estimated by maximizing the likelihood function [19]:

$$J(f_x, f_y) = \left| \sum_{x=M-(W_x-1)/2}^{M+(W_x-1)/2} \sum_{y=N-(W_y-1)/2}^{N+(W_y-1)/2} z(x, y) \exp[-j \cdot 2\pi(f_x x + f_y y)] \right|, \quad (4)$$

with  $W_x$  and  $W_y$  being the estimated window sizes along the  $x$  and  $y$  directions, respectively.

The window size can be adjusted according to a given terrain. For a flat terrain, the interference fringes are sparser and, therefore, larger windows can be used. The interference fringes for a steep terrain are denser so that smaller windows must be used. In this study we choose the window size equal to  $13 \times 13$ .

When the local interference fringes are estimated, a  $32 \times 32$ -point two-dimensional Fourier transform is performed inside the window. In this way a maximum value for the complex two-dimensional phase spectrum is found in the corresponding window. When the local frequency estimation falls within the main lobe of the two-dimensional spectrum, a  $128 \times 128$ -point two-dimensional CZT can be used for spectral refinement.

## 2.3. Phase-unwrapping method based on phase-gradient estimation and energy equation

The basic principle of the phase-unwrapping method based upon the energy equation is to convert the unwrapping constraints into the energy equation. Then a dynamic system based on the energy equation is introduced for minimizing the energy-equation value [15]. The energy equation based on eight neighbourhoods is given by

$$\begin{cases} E_1 = \sum_{i,j} [(\hat{\phi}_{i-1,j} - \hat{\phi}_{i,j})^2 - \cos(\phi_{i,j} - \hat{\phi}_{i-1,j})], & E_2 = \sum_{i,j} [(\hat{\phi}_{i,j-1} - \hat{\phi}_{i,j})^2 - \cos(\phi_{i,j} - \hat{\phi}_{i,j-1})], \\ E_3 = \sum_{i,j} [(\hat{\phi}_{i+1,j} - \hat{\phi}_{i,j})^2 - \cos(\phi_{i,j} - \hat{\phi}_{i+1,j})], & E_4 = \sum_{i,j} [(\hat{\phi}_{i,j+1} - \hat{\phi}_{i,j})^2 - \cos(\phi_{i,j} - \hat{\phi}_{i,j+1})], \\ E_5 = \sum_{i,j} [(\hat{\phi}_{i-1,j+1} - \hat{\phi}_{i,j})^2 - \cos(\phi_{i,j} - \hat{\phi}_{i-1,j+1})], & E_6 = \sum_{i,j} [(\hat{\phi}_{i+1,j+1} - \hat{\phi}_{i,j})^2 - \cos(\phi_{i,j} - \hat{\phi}_{i+1,j+1})], \\ E_7 = \sum_{i,j} [(\hat{\phi}_{i-1,j-1} - \hat{\phi}_{i,j})^2 - \cos(\phi_{i,j} - \hat{\phi}_{i-1,j-1})], & E_8 = \sum_{i,j} [(\hat{\phi}_{i+1,j-1} - \hat{\phi}_{i,j})^2 - \cos(\phi_{i,j} - \hat{\phi}_{i+1,j-1})], \end{cases} \quad (5)$$

$$E_{total} = E_1 + E_2 + E_3 + E_4 + E_5 + E_6 + E_7 + E_8, \quad (6)$$

where  $\phi_{i,j}$  and  $\hat{\phi}_{i,j}$  are respectively the wrapped and unwrapped phases. It is evident that Eq. (6) represents a sum of eight energy equations. Since we deal with the non-path-following method, only  $E_1, E_2, E_3, E_4, E_5, E_6, E_7$  and  $E_8$  are the smallest.

A minimum in Eq. (5) can be obtained by applying the dynamic system along the down energy-gradient direction. The corresponding dynamic system is as follows:

$$\left\{ \begin{array}{l} \frac{d\hat{\phi}_{i,j}}{dt} = -\eta \frac{\partial E_1}{\partial \hat{\phi}_{i-1,j}}, \quad \frac{d\hat{\phi}_{i,j}}{dt} = -\eta \frac{\partial E_2}{\partial \hat{\phi}_{i,j-1}}, \\ \frac{d\hat{\phi}_{i,j}}{dt} = -\eta \frac{\partial E_3}{\partial \hat{\phi}_{i+1,j}}, \quad \frac{d\hat{\phi}_{i,j}}{dt} = -\eta \frac{\partial E_4}{\partial \hat{\phi}_{i,j+1}}, \\ \frac{d\hat{\phi}_{i,j}}{dt} = -\eta \frac{\partial E_5}{\partial \hat{\phi}_{i-1,j+1}}, \quad \frac{d\hat{\phi}_{i,j}}{dt} = -\eta \frac{\partial E_6}{\partial \hat{\phi}_{i+1,j+1}}, \\ \frac{d\hat{\phi}_{i,j}}{dt} = -\eta \frac{\partial E_7}{\partial \hat{\phi}_{i-1,j-1}}, \quad \frac{d\hat{\phi}_{i,j}}{dt} = -\eta \frac{\partial E_8}{\partial \hat{\phi}_{i+1,j-1}} \end{array} \right. , \quad (7)$$

with  $\eta$  representing the convergence rate for our system. Eq. (7) relates the unwrapped phase at the point  $(i, j)$  to the energy-change rate in its neighbourhood.

After substituting Eq. (7) into Eq. (5), discretizing Eq. (5) in time and adding the estimated phase gradients  $\Delta_{i,j}^x$  and  $\Delta_{i,j}^y$ , one can arrive at the relations

$$\left\{ \begin{array}{l} \hat{\phi}_{i,j}^{t+1} = \hat{\phi}_{i,j}^t + \tau [2(\hat{\phi}_{i-1,j}^t - \hat{\phi}_{i,j}^t) + \sin(\phi_{i,j} - \hat{\phi}_{i-1,j}^t)] + \Delta_{i,j}^x, (i = 0, 1, \dots, N) \\ \hat{\phi}_{i,j}^{t+1} = \hat{\phi}_{i,j}^t + \tau [2(\hat{\phi}_{i,j-1}^t - \hat{\phi}_{i,j}^t) + \sin(\phi_{i,j} - \hat{\phi}_{i,j-1}^t)] + \Delta_{i,j}^x, (i = 0, 1, \dots, N) \\ \hat{\phi}_{i,j}^{t+1} = \hat{\phi}_{i,j}^t + \tau [2(\hat{\phi}_{i+1,j}^t - \hat{\phi}_{i,j}^t) + \sin(\phi_{i,j} - \hat{\phi}_{i+1,j}^t)] + \Delta_{i,j}^x, (i = 0, 1, \dots, N) \\ \hat{\phi}_{i,j}^{t+1} = \hat{\phi}_{i,j}^t + \tau [2(\hat{\phi}_{i,j+1}^t - \hat{\phi}_{i,j}^t) + \sin(\phi_{i,j} - \hat{\phi}_{i,j+1}^t)] + \Delta_{i,j}^x, (i = 0, 1, \dots, N) \\ \hat{\phi}_{i,j}^{t+1} = \hat{\phi}_{i,j}^t + \tau [2(\hat{\phi}_{i-1,j+1}^t - \hat{\phi}_{i,j}^t) + \sin(\phi_{i,j} - \hat{\phi}_{i-1,j+1}^t)] + \frac{1}{2}(\Delta_{i,j}^x + \Delta_{i,j}^y), (i = 0, 1, \dots, N) . \\ \hat{\phi}_{i,j}^{t+1} = \hat{\phi}_{i,j}^t + \tau [2(\hat{\phi}_{i+1,j+1}^t - \hat{\phi}_{i,j}^t) + \sin(\phi_{i,j} - \hat{\phi}_{i+1,j+1}^t)] + \frac{1}{2}(\Delta_{i,j}^x + \Delta_{i,j}^y), (i = 0, 1, \dots, N) \\ \hat{\phi}_{i,j}^{t+1} = \hat{\phi}_{i,j}^t + \tau [2(\hat{\phi}_{i-1,j-1}^t - \hat{\phi}_{i,j}^t) + \sin(\phi_{i,j} - \hat{\phi}_{i-1,j-1}^t)] + \frac{1}{2}(\Delta_{i,j}^x + \Delta_{i,j}^y), (i = 0, 1, \dots, N) \\ \hat{\phi}_{i,j}^{t+1} = \hat{\phi}_{i,j}^t + \tau [2(\hat{\phi}_{i+1,j-1}^t - \hat{\phi}_{i,j}^t) + \sin(\phi_{i,j} - \hat{\phi}_{i+1,j-1}^t)] + \frac{1}{2}(\Delta_{i,j}^x + \Delta_{i,j}^y), (i = 0, 1, \dots, N) \end{array} \right. \quad (8)$$

In Eq. (8),  $\tau$  implies the convergence-rate constant and  $\tau < 1$ . The convergence condition for Eq. (8) is given by  $\hat{\phi}_{i,j}^{t+1} = \hat{\phi}_{i,j}^t$ , where  $\hat{\phi}_{i,j}^{t+1}$  and  $\hat{\phi}_{i,j}^t$  are the unwrapped phases at the time moments  $t+1$  and  $t$ , respectively.

### 3. Experimental results and their analysis

#### 3.1. First data-simulation experiment

A simulated phase map with the size of  $100 \times 100$  pixels is shown in Fig. 1. Fig. 2 and Fig. 3 display respectively the interferogram corresponding to Fig. 1 and the same interferogram with the coherence coefficient 0.8. Finally, Fig. 4 shows the unwrapped-phase maps obtained using our method, the network-flow one and the least-squares method. It is seen from Fig. 4 that the

unwrapped-phase map obtained with our method is basically consistent with the original surface, except for a deviation of the centre position. The phase value at the highest point is the same as that of the original surface, whereas the entire unwrapped-phase map is smooth. Although the map obtained from the network-flow method at the highest point is roughly the same as that in the original surface, one observes some burrs in the unwrapped data. On the other hand, the least-squares method yields in multiple burrs, while the highest value is significantly lower than that in the original surface. Therefore the corresponding unwrapped-phase map is less accurate.

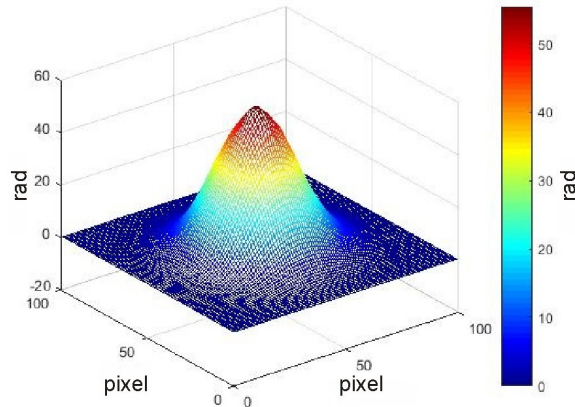


**Fig. 1.** Original phase map.

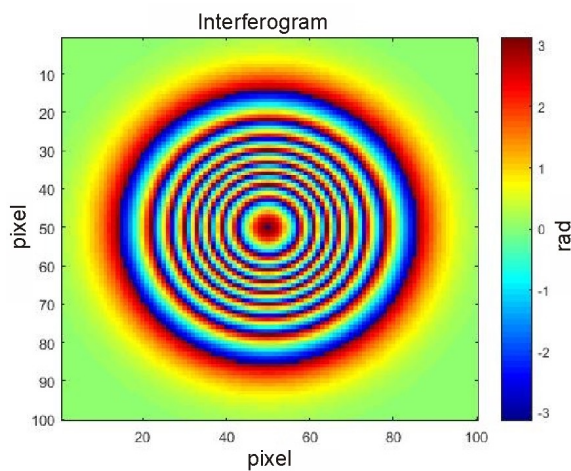


**Fig. 2.** Interferogram with no noise corresponding to Fig. 1.

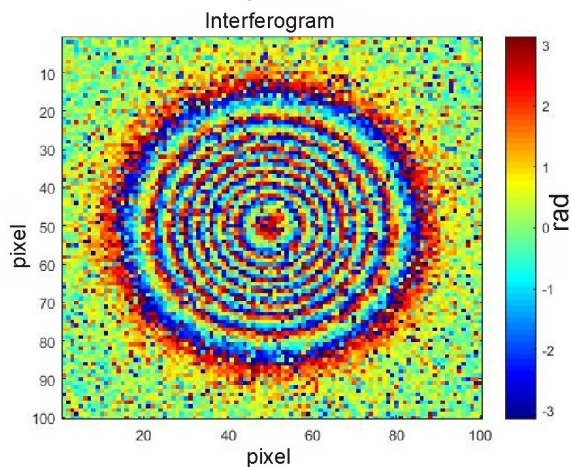


**Fig. 3.** Noisy interferogram corresponding to Fig. 1.

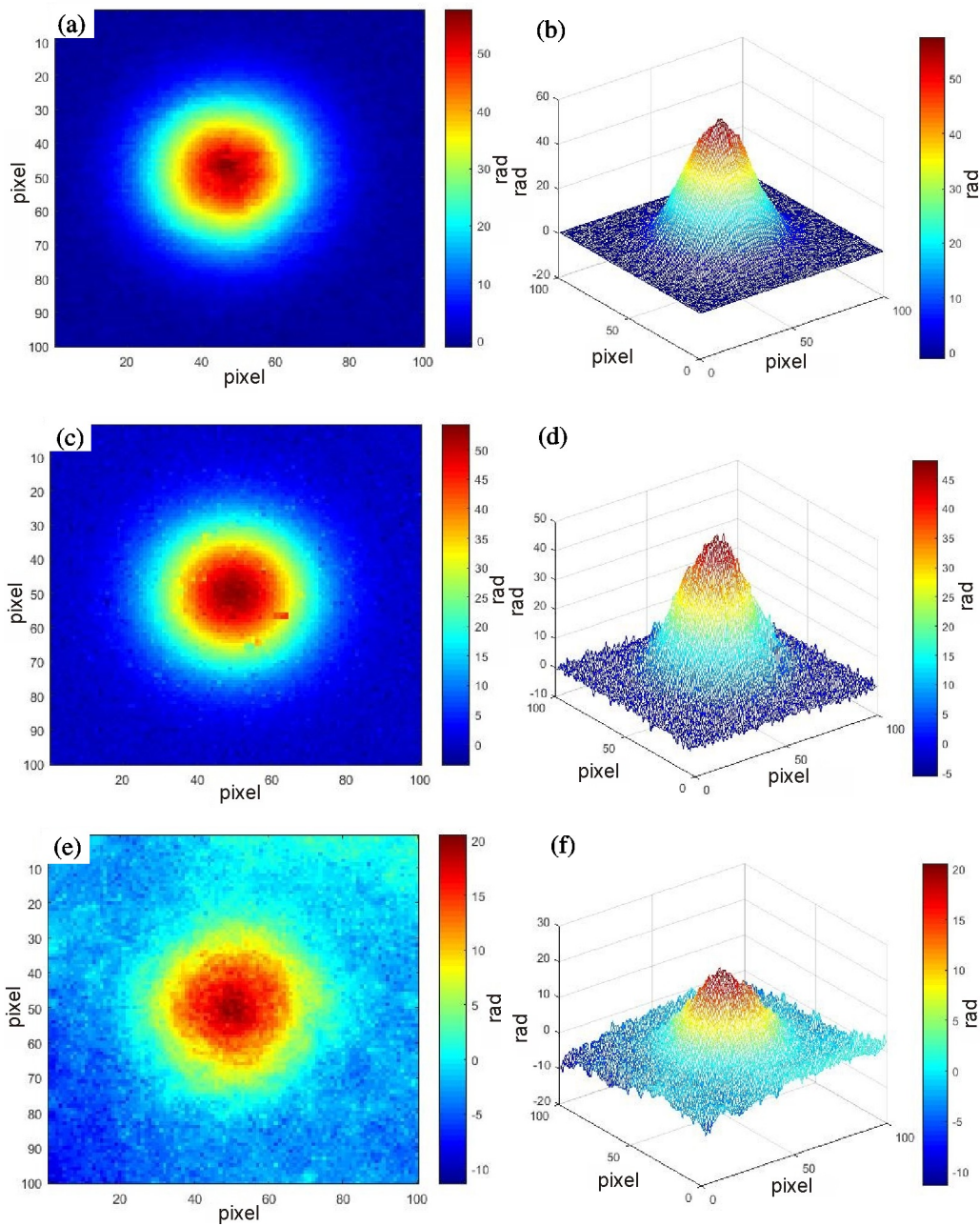


**Fig. 4.** Unwrapped phase maps (panels a, c and e) and three-dimensional maps (panels b, d and f) corresponding to Fig. 1, as obtained by our method (a, b), network-flow method (c, d) and least-squares method (e, f).

In Fig. 5 we show a tenth-row curve obtained from the simulated data. It is obvious that all of the three methods basically reach the maximum value of the original surface. However, the position of the maximum value derived from the least-squares method does not match that of the original surface and its precision is less. Regarding the smoothness of the curves, the least-squares and network-flow methods produce more sawtooth-like curves which manifest higher fluctuations. On the contrary, our method yields the curve which is roughly the same as that corresponding to the original surface, while the unwrapped-phase map is better.

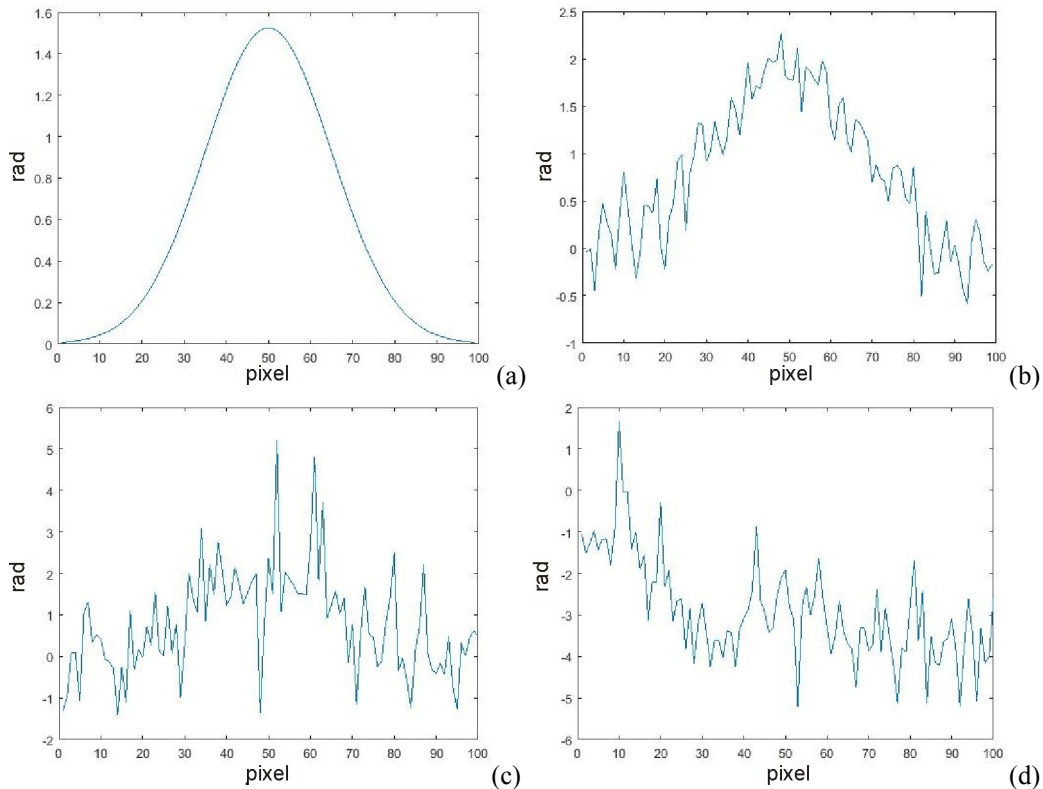


**Fig. 5.** Curves corresponding to the tenth-row phase (see the text): (a) original surface, (b) our method, (c) network-flow method and (d) least-squares method.

### 3.2. Second data-simulation experiment

Now we select for simulations an interferogram with no interference fringes in the upper part and intense interference fringes in its lower part (see Fig. 6). In Fig. 7, we add the Gaussian noise with the coherence coefficient 0.9. It follows from the unwrapped-phase maps shown in Fig. 8 that the method offered in the present work has only insignificant burrs, which are located at the bottom of the three-dimensional map. The amplitude in the part with no interference fringes is the same as that of the original interferogram. Moreover, we obtain in general a better unwrapped-phase map. Concerning the map resulted from the network-flow method, the unwrapped surface is broken and the amplitude corresponding to a non-striped part is obviously lower than that of the original interferogram. Moreover, the latter map involves larger errors. Finally, the map obtained by the least-squares method is too smooth and does not maintain the characteristics of the original surface. The appropriate unwrapped-phase map reveals the largest errors.

The root-mean-square errors associated with the three methods are reported in Table 1. These parameters have been derived when unwrapping a noisy interferogram with different coherence coefficients. Notice also that the root-mean-square errors have been found on the same data and computed from 30 simulations, in order to compare in a fair way the phase-unwrapped results delivered by each method. It is clear from Table 1 that the root-mean-square error calculated for the unwrapped results increases gradually with decreasing coherence coefficient. The error found for our method is the smallest and the precision of the corresponding unwrapped-phase map is the highest. The least-squares method has a larger root-mean-square error due to its peculiar characteristics, while the appropriate unwrapped-phase map is less precise.

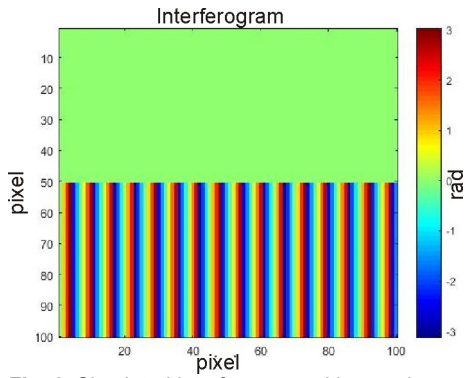


Fig. 6. Simulated interferogram with no noise.

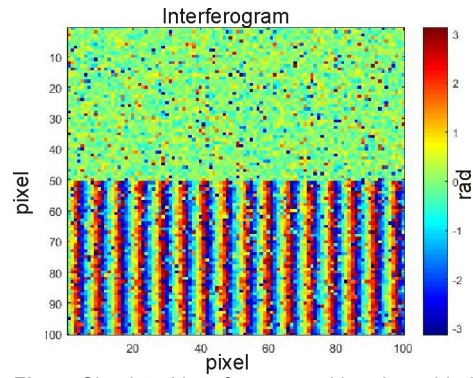
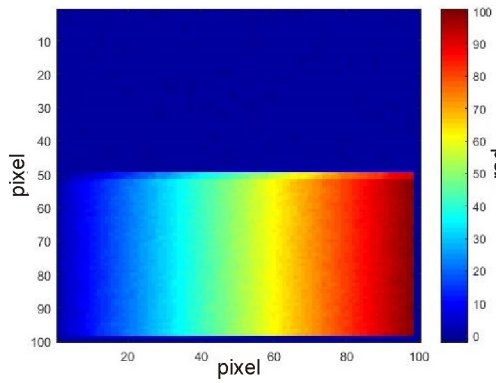
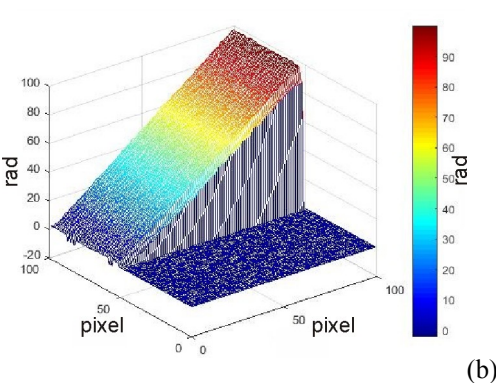


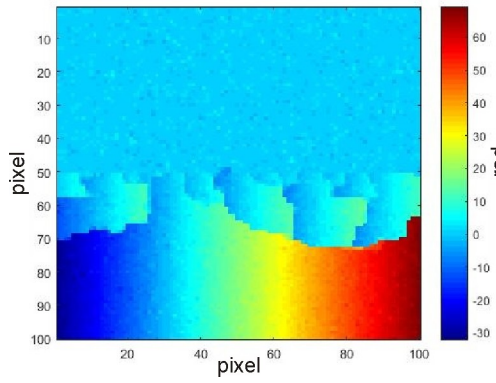
Fig. 7. Simulated interferogram with noise added.



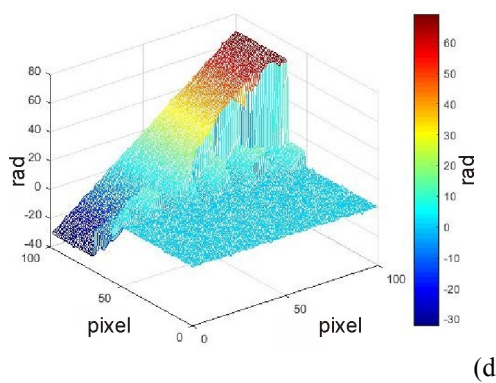
(a)



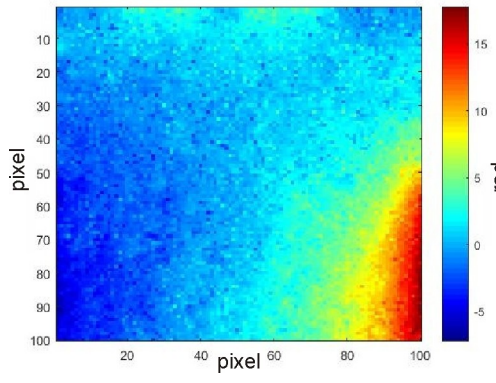
(b)



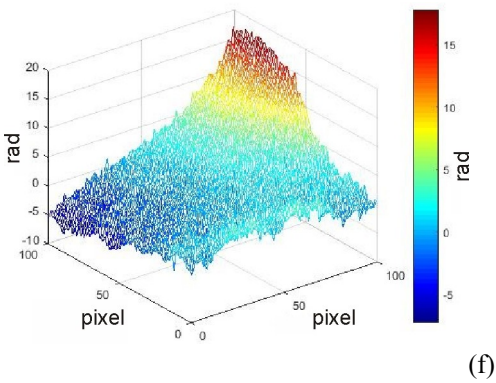
(c)



(d)



(e)



(f)

Fig. 8. Unwrapped phase maps (panels a, c and e) and three-dimensional maps (panels b, d and f) corresponding to Fig. 6 and Fig. 7, as obtained by our method (a, b), network-flow method (c, d) and least-squares method (e, f).

**Table 1.** Comparison of accuracies of the simulated data obtained with different phase-unwrapping methods.

Coherence coefficient	Root-mean-square error of the phase-unwrapping method, rad		
	Our method	Least-squares method	Network-flow method
1.0	0.4079	1.3360	1.3069
0.9	0.8251	1.3385	1.3119
0.8	0.8966	1.3617	1.3323
0.7	1.0825	1.3732	1.3698
0.6	1.2837	1.4629	1.3895
0.5	1.3902	1.5691	1.4207

### 3.3. Real-data experiment

In this Subsection, we perform phase unwrapping on a real interferogram in order to elucidate better the performance of our algorithm and compare it with its counterparts. The experiments have been carried out using a Bam area images in Iran. They have been obtained by the ENVISAT satellite on December 3, 2003 and January 7, 2004. A part of the corresponding interferogram ( $200 \times 200$  pixels – see Fig. 9) has been selected as our experimental data. Examination of the unwrapped-phase maps (see Fig. 10) evidences that there are many glitches in the three-dimensional unwrapped-phase map obtained using the network-flow method. There is an error for the highest phase value derived in the three-dimensional unwrapped-phase map using the least-squares method. This indicates that the corresponding errors are too large. On the contrary, due to phase-gradient estimation, our method provides satisfactory results even when there are many fringes. It manifests a higher phase-unwrapping precision and, moreover, the error propagation is prevented.

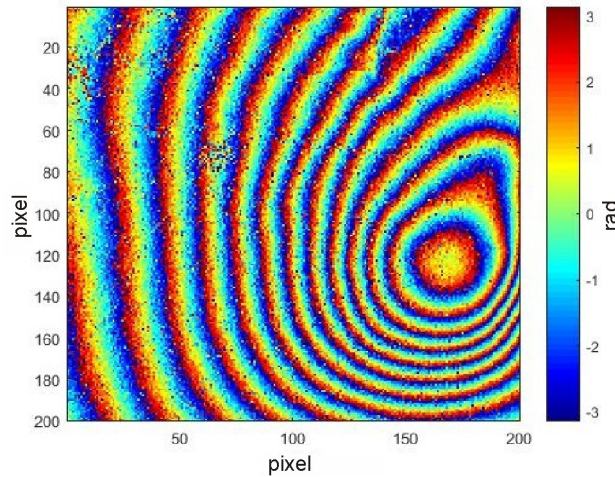


**Fig. 9.** Experimental interferogram

A point where the absolute difference value between the adjacent pixels' phase gradients exceeds  $\pi$  is a so-called 'discontinuity point', whereas a map generated by the discontinuity points is termed as a 'discontinuity map' [19]. In real-data experiments, the unwrapped-phase maps are usually analyzed qualitatively. If the distribution of discontinuity points is dense, this means that the phase-unwrapping algorithm reveals poor performance in preventing error propagation.

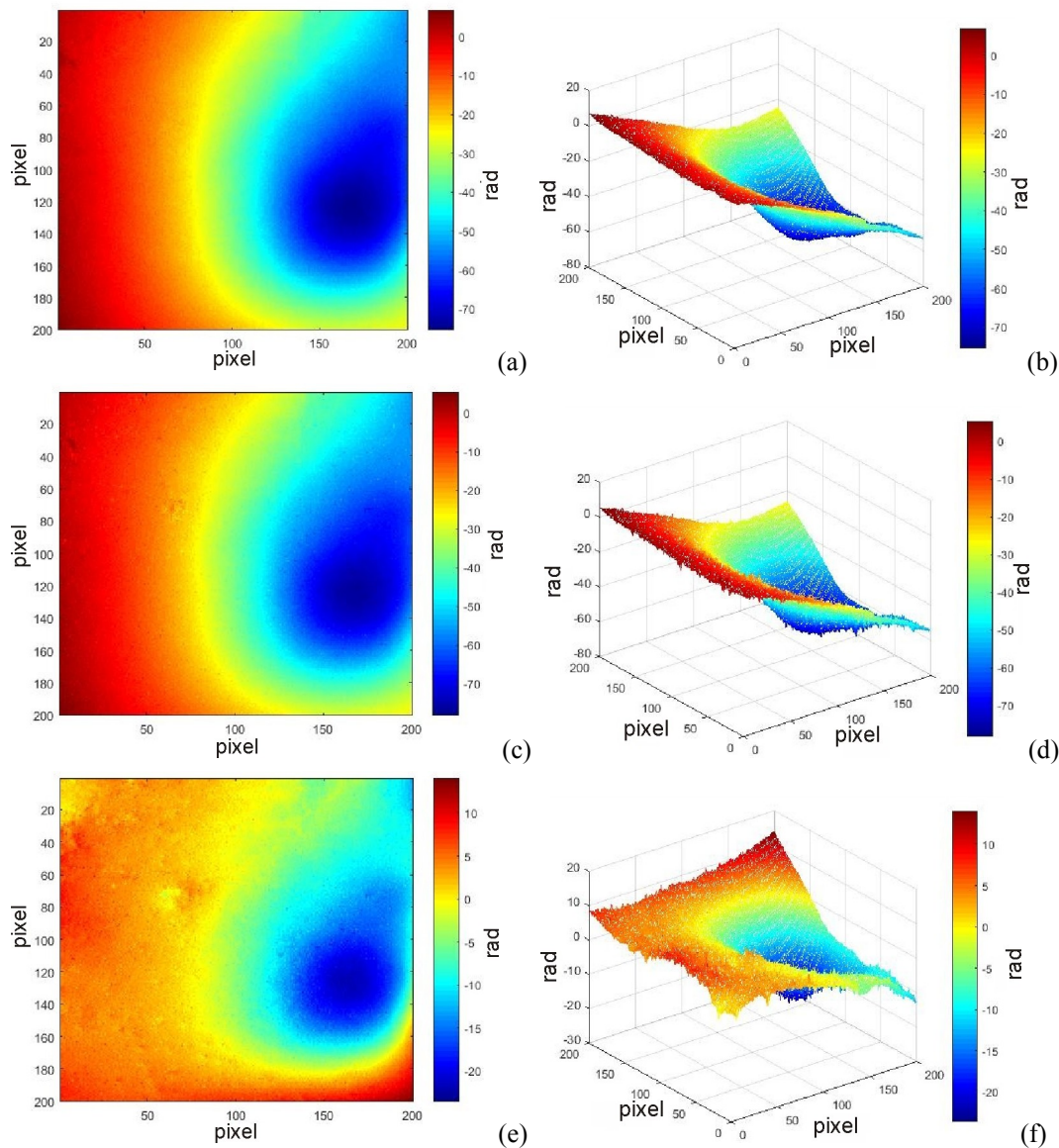


**Fig. 10.** Unwrapped phase maps (panels a, c and e) and three-dimensional maps (panels b, d and f) corresponding to real data (see experimental interferogram in Fig. 9), as obtained by our method (a, b), network-flow method (c, d) and least-squares method (e, f).

When analyzing the discontinuity map corresponding to the original interferogram (see Fig. 11a), one can see that the discontinuity points for the experimental data are distributed mainly at the fringe edges and there are only two dense discontinuities in the upper left corner. Fig. 11b displays the discontinuity map typical for our method. There are no discontinuity points in the whole map, which indicates that our method can efficiently limit the local errors. The discontinuity map for the network-flow method (see Fig. 11c) reveals that this method is less resistible with respect to the error propagation. Finally, the discontinuity map typical for the least-squares method (see Fig. 11d) shows that the number of discontinuity points is significantly reduced, if compared with the method mentioned above. In other words, this approach also reveals some resistibility to the error-propagation effect.

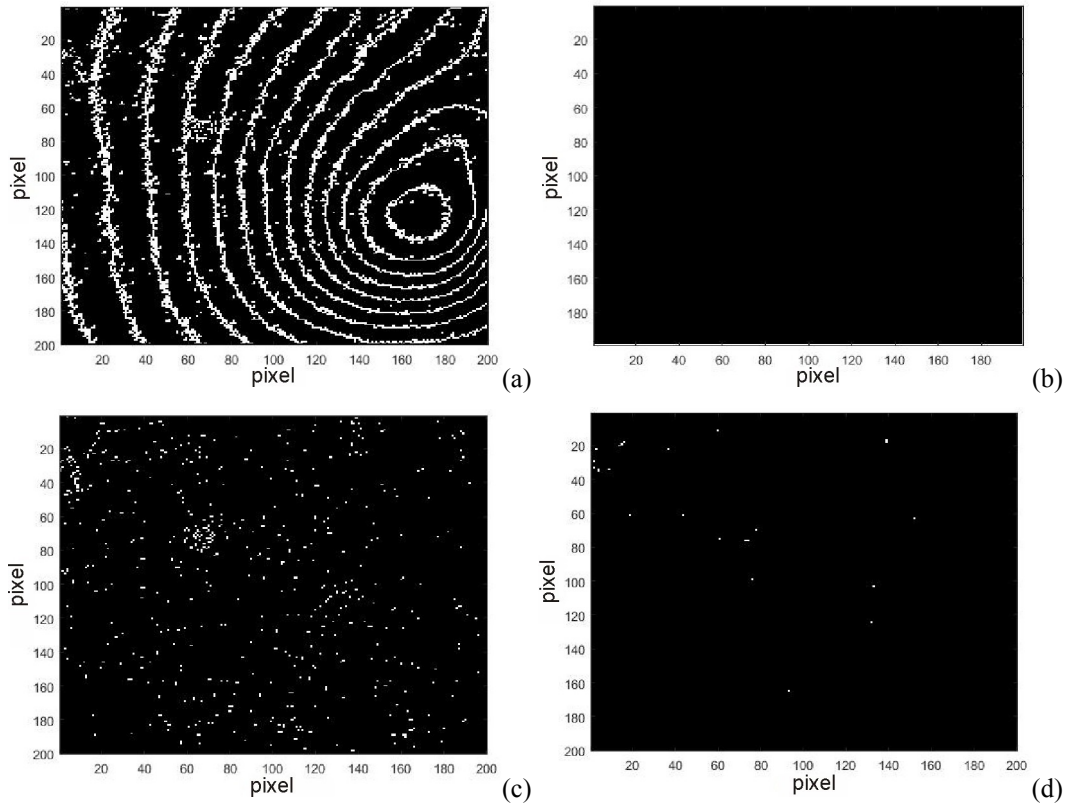


**Fig. 11.** Discontinuity maps corresponding to original interferogram (a), our method (b), network-flow method (c) and least-squares method (d).

In order to check the unwrapping errors in a more detail, the unwrapped results have been rewrapped to generate so-called rewrapped maps [20]. As seen from Fig. 12, the rewrapped-fringe pattern corresponding to our method remains consistent with that of the original fringe pattern. If compared with the original fringe pattern, the least-squares method also reveals less dispersion of speckle noise in the rewrapped data. On the contrary, the fringe patterns associated with the least-squares method are essentially lost and the unwrapping errors are larger. Summing up this analysis, we conclude that our method unwraps successfully the wrapped phase and, moreover, it removes efficiently the phase noise contained in the wrapped-phase images.

To measure the quality of unwrapped data, a so-called  $\varepsilon$  value is often used [21]. The smaller the  $\varepsilon$  value, the higher the unwrapping quality is. The  $\varepsilon$  parameter can be calculated as

$$\varepsilon = \frac{1}{MN} \sum_{i=0}^{M-2} \sum_{j=0}^{N-1} \omega_{i,j}^x \left| \varphi_{i+1,j} - \varphi_{i,j} - \Delta_{i,j}^x \right|^p + \frac{1}{MN} \sum_{i=0}^{M-1} \sum_{j=0}^{N-2} \omega_{i,j}^y \left| \varphi_{i,j+1} - \varphi_{i,j} - \Delta_{i,j}^y \right|^p, \quad (9)$$

where  $M$  and  $N$  are the numbers of respectively columns and rows,  $\varphi_{i,j}$  is the unwrapped phase at the point  $(i, j)$ , and  $\omega_{i,j}^x$  and  $\omega_{i,j}^y$  denote the weights corresponding respectively to the wrapped-phase gradients  $\Delta_{i,j}^x$  and  $\Delta_{i,j}^y$ . Some weight is generally given to the phase-quality map, with its value being in general between 0 and 1, while the  $p$  value is usually taken to be 0, 1 or 2. In our case, we put the  $p$  parameter to be equal to 1.

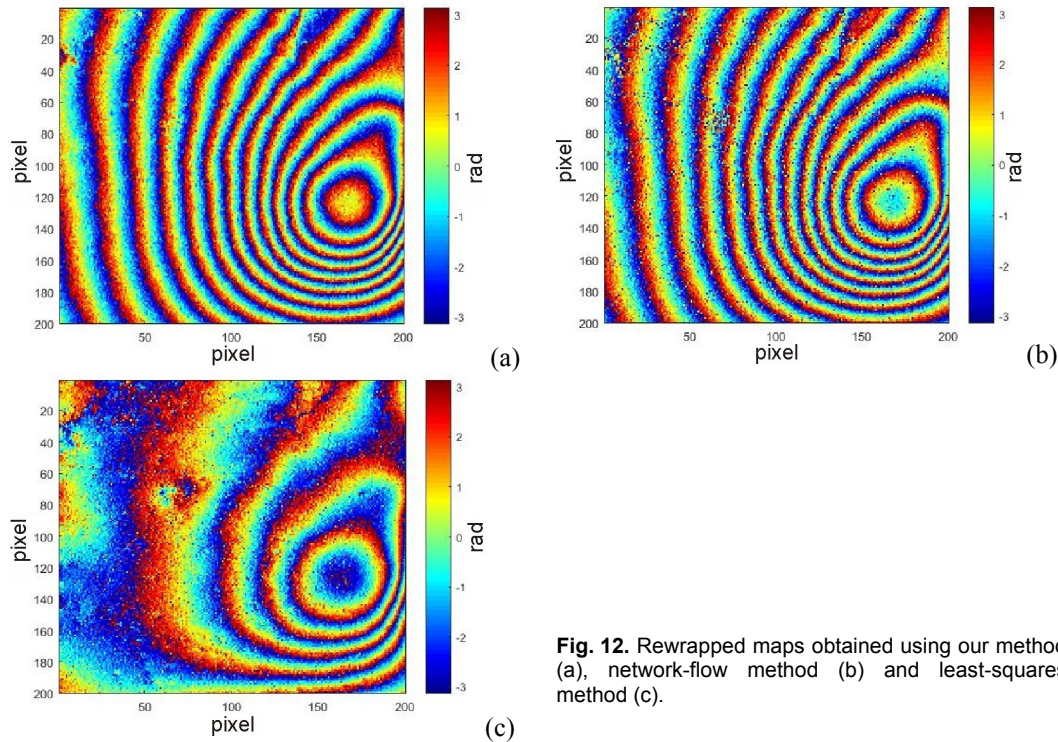


**Fig. 12.** Rewrapped maps obtained using our method (a), network-flow method (b) and least-squares method (c).

As seen from Table 2, the number of discontinuity points peculiar for our method is significantly less than those of the network-flow and least-squares methods, thus indicating that our unwrapped results are more reliable. The  $\varepsilon$  value for our method is slightly less than those typical for the other two methods so that the quality of our unwrapped-phase map is higher. Finally, the root-mean-square and median errors corresponding to our method are the lowest. This implies that the accuracy of unwrapping performed by our method is the highest.

**Table 2.** Comparison of accuracy parameters obtained for different phase-unwrapping methods applied to real experimental data.

Phase-unwrapping method	Number of discontinuity points	$\varepsilon$ value	Root-mean-square error	Average error
Our method	0	0.7293	0.6294	0.6572
Network-flow method	638	0.7410	1.3849	3.5451
Least-squares method	25	0.8151	1.5013	3.5022

#### 4. Conclusion

In this work we offer a robust phase-unwrapping method based on the estimation of phase gradient and energy equation. It retrieves continuous phase maps from interferograms, using a highly efficient phase-gradient estimation. The results obtained from both simulated and real experimental phase data demonstrate high enough efficiency of our method. In particular, a comparison with the commonly used methods, including the network-flow and least-squares ones, demonstrates that the approach suggested by us limits propagation of errors in the phase-unwrapping process to a certain extent and provides more accurate final data. As a consequence, the results obtained in the present work would suggest new ideas for data processing performed with the InSAR technique.

---

## Acknowledgement

This work was supported by the Natural Science Foundation of Shandong Province, China (the Grant #ZR2019PF023) and the Science and Technology Development Plan Project of Weifang City (the Grant #2019GX005).

## References

1. Goldstein R M, Zebker H A and Werner C L, 1988. Satellite radar interferometry: two-dimensional phase unwrapping. *Radio Sci.* **23**: 713–720.
2. Fornaro G, Franceschetti G, Lanari R and Sansosti E, 1996. Robust phase-unwrapping techniques: a comparison. *J. Opt. Soc. Amer. A.* **13**: 2355–2366.
3. Yang L, Liu W and Zhao Y J, 2007. Branch-cut strategy analyses in phase unwrapping algorithm for interferometric SAR. *Sci. Surv. Mapp.* **3**: 75–77.
4. Fornaro G and Sansosti E, 1999. A two-dimensional region growing least squares phase unwrapping algorithm for interferometric SAR processing. *IEEE Trans. on GRS.* **37**: 2215–2226.
5. Wang C, Zhang H and Liu Z. *Spaceborne synthetic aperture radar interferometry*. Beijing: Science Press, 2002.
6. Flynn T J, 1996. Consistent 2-D phase unwrapping guided by a quality map. *Geosci. Remote Sens. Symp.* **1**: 2057–2059.
7. Flynn T J, 1997. Two dimensional phase unwrapping with minimum weighted discontinuity. *J. Opt. Soc. Amer. A.* **14**: 2692–2701.
8. Pritt M D, 1997. Phase unwrapping by means of multigrid techniques for interferometric SAR. *IEEE Trans. GRS.* **34**: 728–738.
9. Zebker H A and Lu Y, 1998. Phase unwrapping algorithms for radar interometry: residue-cut, least-squares, and synthesis algorithms. *J. Opt. Soc. Amer. A.* **15**: 586–598.
10. Gao Y, 2000. On InSAR 2D phase unwrapping algorithm. *Geogr. Territ. Res.* **16**: 90–96.
11. Xu W and Cumming I, 1999. A region-growing algorithm for InSAR phase unwrapping. *IEEE Trans. GRS.* **37**: 124–133.
12. Fornaro G, Franceschetti G and Lanari R, 1997. Interferometric SAR phase unwrapping using Green's formulation. *IEEE Trans. GRS.* **34**: 720–727.
13. Zhan Zongqian, Qian Jun, Shu Ning, 2002, A Method of Phase Unwrapping Based on Region-segmentation and Encoding. *Geomatics and Information Science of Wuhan University*, **27**(3): 316-320.
14. Massonnet D, Vadon H and Rossi M, 1996. Reduction of the need for phase unwrapping in radar interferometry. *IEEE Trans. Geosci. Remote Sens.* **34**: 489–497.
15. Servin M and Rodriguez R, 1994. A robust cellular processor for phase unwrapping. *J. Mod. Opt.* **41**: 119–127.
16. Liming Pu, Xiaoling Zhang, Zenan Zhou, Liang Li, Liming Zhou, Jun Shi and Shunjun Wei, 2021. A robust InSAR phase unwrapping method via phase gradient estimation network. *Remote Sens.* **13**: 45–64.
17. Xie X M and Li Y H, 2014. Enhanced phase unwrapping algorithm based on unscented Kalman filter, enhanced phase gradient estimator, and path-following strategy. *Appl. Opt.* **53**: 4049–4060.
18. Liu J G, Wang J F, Wang Z L and Liu W K, 2018. A new method of InSAR phase unwrapping processing considering the terrain factors. *IWEMSE.* 672–680.

- 
19. Spagnolini U, 1995. 2-D phase unwrapping and instantaneous frequency estimation. IEEE Trans. GRS. **33**: 579–589.
  20. Hao H D. Study of Kalman filter applied in phase unwrapping of InSAR. Qing Dao: Master of Philosophy from Shandong University of Science and Techology, 2010.
  21. Gao J, Kosaka A and Kak AC, 2005. A multi-Kalman filtering approach for video tracking of human-delineated objects in cluttered environments. Computer Vision and Image Understanding. **99**: 1–7.
  22. Guo H D, 1997. Spaceborne multifrequency, polarimetric and interferometric radar for detection of the targets on Earth surface and subsurface. J. Remote Sens. **1**: 32–39.

---

Man Yan, Juanjuan Luo and Defa Hu. 2022. Phase-unwrapping method based on phase-gradient estimation and energy equation. Ukr.J.Phys.Opt. **23**: 201 – 214.

doi: 10.3116/16091833/23/4/201/2022

***Анотація.** Розгортання фази – це ключовий крок в обробці даних інтерферометричних радарів із синтетичною апертурою (InSAR). Ми пропонуємо метод фазового розгортання, заснований на оцінюванні градієнта фази та енергетичному рівнянні. Цей метод можна реалізувати шляхом коригування чотирьох околиць у вихідному методі енергетичного рівняння до восьми околиць і поєднанні швидкого перетворення Фур'є та перетворення Chirp-Z для оцінки градієнта фази в ітераційному рівнянні. Для проведення експериментів із розгортанням фази використано змодельовані та реальні дані InSAR. Метод розгортання фази на основі оцінки градієнта фази та енергетичного рівняння протестовано за допомогою таких кількісних стандартів як, наприклад, карта розривів і середньоквадратична похибка. На цій основі виконано порівняння нашого підходу з деякими іншими стандартними методами розгортання фази. Показано, що запропонований метод ефективно пригнічує помилки, які виникають у процесі розгортання фази, і дає надійні та високоточні результати розгортання.*